Molecular modeling and simulations of some antiviral drugs, benzylisoquinoline alkaloid, and coumarin molecules to investigate the effects on Mpro main viral protease inhibition

Showkat Ahmad Mir [a],[*], Rajesh Kumar Meher [b], Binata Nayak [a],[**]

[a] *School of Life Sciences, Sambalpur University, Jyoti Vihar, Odisha, 768019, India*
[b] *Advance Centre for Treatment, Research, and Education in Cancer, Tata Memorial Centre, Mumbai, India*

A B S T R A C T

Background: SARS-CoV-2 is a deadly viral disease and uncounted deaths occurs since its first appearance in the year 2019. The antiviral drugs, benzylisoquinoline alkaloids, and coumarin molecules were searched using different online engines for drug repurposing with SARS-CoV-2 and to investigate the effects on main viral protease (Mpro) upon their bindings.
Methods: A database composed of antiviral drugs, benzylisoquinoline alkaloids, and Coumarin molecules was screened through a molecular docking strategy to uncover the interactions of collected molecules with SARS-CoV-2 Mpro. Further, molecular dynamics simulations (MDS) were implemented for 100 ns to calculate the stability of the best complexed molecular scaffold with Mpro. The conformations of the simulated complexes were investigated by using principal component analysis (PCA) and Gibbs energy landscape (FEL) and DSSP together. Next, free binding energy (ΔG_{bind}) was calculated using the *mmpbsa* method.
Results: Molecular docking simulations demonstrate 17 molecules exhibited better binding affinity out of 99 molecules present in the database with the viral protease Mpro, followed ADMET properties and were documented. The Coumarin-EM04 molecular scaffold exhibited interactions with catalytical dyad HIS41, CYS145, and neighboring amino acids SER165 and GLN189 in the catalytical site. The crucial factor RMSD was calculated to determine the orientations of Coumarin-EM04. The Coumarin-EM04 complexed with Mpro was found stable in the binding site during MDS. Furthermore, the free energy binding ΔG_{bind} of Coumarin-EM04 was found to be -187.471 ± 2.230 kJ/mol, and for Remdesivir ΔG_{bind} was -171.926 ± 2.237 kJ/mol with SARS-CoV-2 Mpro.
Conclusion: In this study, we identify potent molecules that exhibit interactions with catalytical dyad HIS41 and CYS145 amino acids and unravel Coumarin-EM04 exhibited ΔG_{bind} higher than Remdesivir against Mpro and thus may serve better antiviral agent against SARS-CoV-2.

1. Introduction

SARS-CoV-2 (COVID-19) is spreading at an alarming rate globally. The numbers of patients are uncountable because of its asymptomatic transmissions [1] and the non-availability of specific drugs. As per the literature review, the SARS-CoV-2 primarily takes space in upper esophageal regions and later occupies the whole thoracic cavity which leads to hypoxia [2]. An insufficient supply of oxygen at the tissue level and henceforth patients need oxygen [3]. The main viral protease of Coronavirus is composed of two identical subunits S1/S2 together forming two active sites a catalytic dyad Cys145 and His41, which

exhibits furin cleavage [4–6]. The catalytic dyad Cys145 and His41 is a primary interest of researchers all over the world to target anyone in a catalytic dyad that may hinder SARS-CoV-2 duplication [7]. However, the spike proteins of SARS-CoV-2 bind with human ACE2 in a similar fashion as that of SARS-CoV [6]. Phylogenetic analysis shows that the newly emerged SARS-CoV-2 share >80% nucleotide identity and 89.1% nucleotide similarity with SARS-CoV and MERS [7,8]. The highly infectious diseases parade social disharmony and leave the 21st century in deep fear. Clinical trials of vaccines and small drug molecules are now the focus of scientific research around the globe, even some vaccines and synthetic drug molecules are undergoing human trials. Again, the very

low effectiveness of pneumonia vaccines against COVID-19 is being reported. Several phytochemicals such as curcuminoids were identified as the better inhibitors confirmed by in-silico investigations against Nsp15 a non-structural protein of the SARS-CoV-2 [9]. Moreover, phytochemicals from the tea plant Theaflavin are more potent and showed lower binding energy than standard molecules against Nsp16 of SARS-CoV-2 [10]. Also, the Oolonghomobisflavan-A and Theasinensin-D phytochemicals were found to be potent inhibitors of SARS-CoV-2 main protease [11]. Subsequently Diacetylcuecumin and Dicaffeoylquinic acid also showed robust interactions with the human ACE2 receptor of SARS-CoV-2 [12]. However, the turmeric-derived compounds showed better bindings with RNA-dependent RNA polymerase of SARS-CoV-2 [13]. More research is needed to identify novel anti-viral agents against SARS-CoV-2 by targeting various therapeutic proteins.

However, there are fewer coumarin molecules that were investigated against SARS-CoV-2, and the present study intended to identify the novel coumarin molecules against SARS-CoV-2. Coumarin molecules are organic compounds found in many plants and herbs. They are used to make a variety of products from perfumes to medicines and health supplements. Coumarins have been found to possess antiviral activities against a variety of viruses, including human immunodeficiency virus (HIV), influenza virus, herpes simplex virus, and hepatitis C virus. Coumarins are also known for their anti-inflammatory and anti-cancer properties. Coumarins constriction in varieties of plants is composed of benzene and alpha-pyrone rings [14,15]. They have diverse pharmacological properties like antiviral, antibacterial, antihypertensive, multiple sclerosis, antiadipogenic, and antioxidant [16–18]. Next, natural coumarins are divided into six types: mostly angular types of natural coumarins show antiviral activity. Noscapine is a benzylisoquinoline alkaloid prescribed as a cough suppressant and exerts antimitotic activity by binding within the interfaces of the tubulin resulting in disruption of microtubule assembly dynamics, inhibits tumor mitosis and has very low toxicity against normal cells [19,20]. Here, 72 derivatives of Coumarins, 5 molecules of Noscapine analogs, and 22 reported antiviral drug molecules, a total of 99 molecules are taken into account to repurpose with the Mpro of SARS-CoV-2 and to investigate the binding nature of the molecules via combined computational approaches since these molecules owing diverse pharmaceutical activity and widely distributed in the nature and were selected in current study because that probably may have anti-COVID-19 activity by targeting Mpro of SARS-CoV-2. Comparative structural analysis of several antiviral drugs, phytochemicals such as coumarins and noscapine derivatives against SARS-CoV-2 to understanding the binding interplay with catalytic dyad and other neighboring amino acids present in the binding site. Also, MD simulations were employed for the best complexes to determine their stability for a long-range simulation run. Moreover, the free binding energy was calculated to determine the binding potential of the identified in this present study.

2. Material and methods

2.1. Preparation of ligands and molecular docking simulations

All the desired ligands were drawn using ChemDraw Ultra 8.0.3 and converted into PDB format using chem3D Ultra 8.0.3 [21]. The molecules were in imported to the database viewer and prepare a database using (MOE.v09) [22,23].

The main viral protease protein PDB ID: 6LU7 was retrieved from the RCBS protein data bank [24]. The molecular docking was carried out by using (MOE.v09) [6]. Proteins were prepared by ignoring water molecules and protonate3D application was used to re-optimize the hydrogen bond network, the dielectric was set at gas phase 1. Partial charges were added and the 6LU7 protein was minimized by using the MMFF94x default force field [22,23]. The catalytical site were selected using Atom Selector application. The triangle matcher was used as a default

placement method for docking. The binding free energy was calculated by Affinity dG scoring functions [25]. Next, the prepared database of phytochemicals including some reported viral drug molecules were selected for free energy estimation with SARS-CoV-2 Mpro. The final 10 ligand poses were minimized in the receptor of the main viral protease of SARS-CoV-2 Mpro and the analysis was done using the LigX module.

2.2. Evaluation of toxicity

Online web servers were used to calculate the molecular property of small molecules. The prediction of compound toxicities is important for drug design. The basic need of the computational toxicity model is to estimate the toxic doses in animals, which helps to reduce the mass utilization of animal models for experiments. The Protox-II [26] was used to evaluate the toxicity of molecules that showed better interaction with the binding pocket of the receptor. The toxicity predictions like LD50 Value, class of toxicity, and toxicity fragments of each molecule were calculated by using Protox-II [26,27]. The molecular property is calculated on a fragment, based on contributions attributed to the structure. The test set of molecules was split into a linear and nonlinear fragment, a partial least squares regression model was built and optimized for a particular property using a leave 50% out cross-validation calculations. This method is robust and very fast, more than 5k or equal to 5k molecules are calculated per second. Open babel [28] is a free software used to generate the smiles format and is used as input data in Protox-II [25–27,29].

2.3. Molecular dynamic simulations and free binding energy assessment

The Gromacs 5.1.1. was used to perform molecular dynamics simulations [30,31]. The water and ligand were removed from the complex. The protein topology was generated using the AMBER99SB-ILDN force field and recommended water model TIP3P [32,33]. The ligand topology was generated from the acpype server and parameters for each bond were assigned using GAFF [34,35]. Both the ligand and protein topologies were incorporated in a single gromacs readable file and then inserted in the 3-dimensional box which is 1 nm apart from the walls of the PBC [36]. The system was solvated using an SPC module by adding 28011 solvents and the retained charges were naturalized using 4 Na^+ ions. The system was equilibrated for 5000 steps using the steepest descent algorithm and coulomb-type PME was used for the treatment of long-range electrostatic interaction [37]. Further, the system was equilibrated with 100 ps in an NPT and NVT ensemble with a velocity-rescaling thermostat and a modified Berendsen barostat [38]. The temperature and pressure were adjusted to 300K and 1 bar respectively. The Coulomb's cut-off scheme was kept at 1.2 nm and long-range electrostatic interactions were handled by the PME algorithm. To constrain the bond length LINICS algorithm was selected [39, 40]. The simulations for each complex were performed by applying a time step of 2 fs for 100 ns simulations at 300 K and 1 atm, under an NPT ensemble with a velocity-rescaling thermostat and Parrinello-Rahman barostat [41], to sustain temperature and pressure close to reference values. Seven simulations were performed in this present study and the results were analyzed using gromacs modules (rmsd, rmsf, sasa, rg, h_bond, h_dist, pca, g_sham and do_dssp).

The Free energy was calculated by the linearized traditional PBE method. Multiple debye-huckle sphere boundary conditions and ionic strength of 0.150 M concentrations were used with default grid dimensions x = 129, y = 129, and z = 97 Å. Nonpolar solvation energy was calculated using solvent accessible surface area (SASA) model. Also, the default values of surface tension of the solvent, and SASA energy constant from previous MM/PBSA calculations of 0.0226778 kJ/mol $Å^2$, and 3.84982 kJ/mol were used respectively [42,43]. Average free energy binding of coumarin-EM04 and remdesivir bound SARS-CoV-2 were performed by using g_mmpbsa [44]. Final 60–70 ns of simulation frames from input files were obtained after the completion of molecular

Table 1
Comparative binding analysis of Antiviral, Alkaloid, and coumarin molecules with Remdesivir against SARS-CoV-2.

Positive Control		SARS-CoV-2 Endocytotic drugs		Antiviral drugs		Benzylisoquinoline alkaloid Molecules		Coumarins	
NAME	Binding energy kcal/ mol	NAME	Binding energy kcal/ mol	NAME	Binding energy kcal/ mol	NAME	Binding energy kcal/ mol	NAME	Binding energy kcal/ mol
Remdesivir	−4.087	Chloroquine	−2.85	Camostat	−4.130	Noscapine	−2.114	Coumarin EM01	−5.142
		Hydroxychloroquine	−1.5367	Fingolimod	−3.470	Bromo-Noscapine	−1.622	Coumarin EM02	−4.487
				Galidesivir	−3.720			Coumarin EM03	−4.362
				Favipiravir	−3.563			Coumarin-EM04	−4.516
				Baloxavir Marboxil	−1.827				
				Laninamivir	−5.776				
				Ribavirin	−4.573				
				Tenuifoliside B	−6.2488				

dynamic simulations and were used for free energy binding calculations thrice. The average free energy binding was calculated by the bootstrap method using MmPbSaStat.py. The decomposition energy of each amino acid contributes to free energy bindings was calculated by the MmPbSaDecomp.py module of *g mmpbsa*. The ΔG_{bind} was calculated according to the following equation (i).

$$\Delta G_{binding} = \Delta G_{complex} - \left(\Delta G_{protein} \right) + \left(\Delta G_{ligand} \right) \tag{i}$$

This method was implemented to calculate the free binding energy of molecular scaffolds with Mpro of SARS-CoV-2 [11,45,46].

2.4. Principal component analysis and free energy landscape analysis

The movement of amino acids to a set of linearly uncorrelated variables is studied using the principal component (PCA) analysis of statistics [47,48]. Next, the covariance matrix and eigenvalues were calculated using the Gromacs package *gmx anaeig*. By diagonalizing the covariance matrix, the eigenvectors are calculated and the associated motions in a sampled system were computed by using the gmx covar module. Finally, PC1 vs PC2 Gibbs energy landscape was calculated by using the *gmx sham* module and *gmx xpm2ps* was used to generate the images.

3. Results and discussion

3.1. Molecular docking studies

The molecular docking study demonstrates that 17 molecules exhibited better interaction with the binding site of SARS-CoV-2 (PDB ID: 6LU7) out of 99 molecules present in the database. However, seventeen different molecules are documented in this article based on their significant binding interactions. Table 1 depicts the binding free energies of these seventeen different molecules with 6LU7. Remdesivir as an antiviral drug is being used for the treatment of COVID-19 developed by Gilead Sciences Inc [49,50]. but holds toxic fragments. Previously, it was used to treat Ebola virus disease as well as against infection of the Marburg virus. Remdesivir, an RNA-dependent RNA polymerase inhibitor stops the duplication of SARS-CoV-2 [51,52]. Hydroxychloroquine and Chloroquine are also used as endocytotic drugs against SARS-CoV-2 but they also show binding affinity with M^{pro} SARS-CoV-19. This reveals that Hydroxychloroquine and Chloroquine have multi-target drug functionality against SARS-CoV-2. Remdesivir was docked with Mpro. The best interacting mode of the binding pocket of the protease (ligand brown, oxygen red, and nitrogen blue) was shown and it was observed that amino acid residues: THR25, SER46, and GLN189 were actively involved in interaction with the ligand through hydrogen bond interactions. THR25 was bound to the amine group of the ligand: Remdesivir, whereas SER46 was bound to oxygen atoms of the furan ring present in the ligand. Besides, GLN189 binds to the
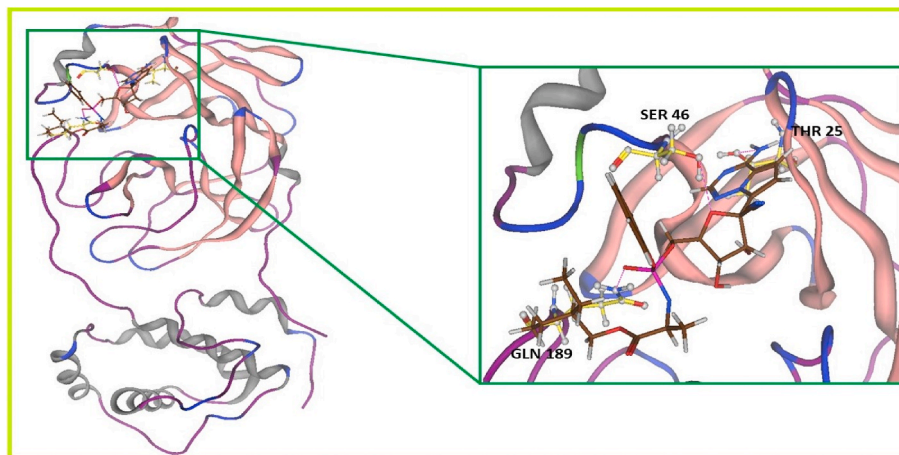

Fig. 1. Remdesivir was docked with the main viral protease of SARS-CoV-2, the interactions exhibited by remdesivir were found with the binding site but no interactions exist with the catalytical dyad HIS 41 and CYS165 amino acids.
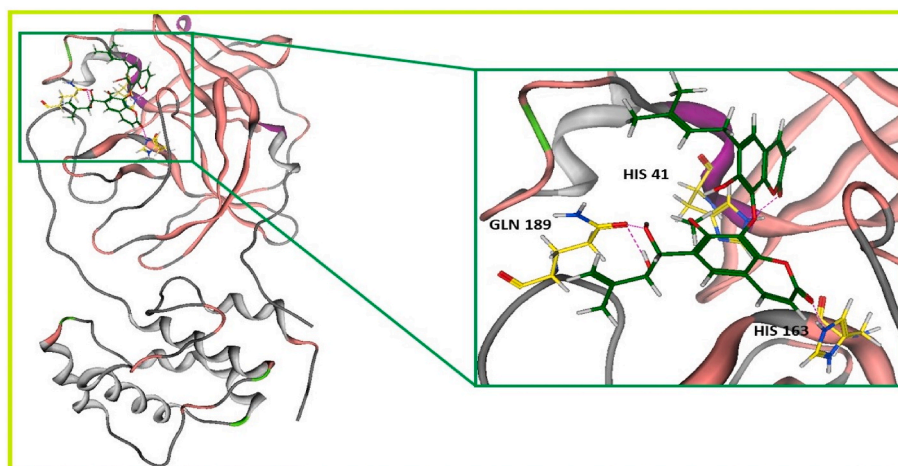
Fig. 2. The docking interactions exhibited by the Coumarin-based molecular scaffold (Coumarin-EM04) IUPAC name 6-(1,2-dihydroxy-3-methylbut-3-enyl)-8-(7-hydroxy-6-(3-methylbut-2-enyl)-2-oxo-2H-chromen-8-yloxy)-7-methoxy-2H-chromen-2-one with HIS41, HIS 163, and GLN 189 with the main viral protease of SARS-CoV-2 Mpro.

Table 2
The interactions exhibited by the ligand with SARS-CoV-2 M^{PRO}, drug-likeness (DL), and toxicity class are given below.

Molecule Name	Interacting amino acids of 6LU7	LD-50 mg/kg	Complex with Mpro
1. Remdesivir	THR25, SER46, GLN189,	1000	Complex with Mpro
2. Chloroquine	GLU166	311	Complex with Mpro
3. Camostat	ASN119, HIS163	3000	Complex with Mpro
4. Fingolimod	PHE140, ASN142, GLU166, HIS163	315	Complex with Mpro
5. Galidesivir	PHE140, LEU141, ASN142, GLN189, HIS163	500	Complex with Mpro
6. Favipiravir	THR45.SER46	555	Complex with Mpro
7. Noscapine 2	SER46, ASN142, GLN189	853	Complex with Mpro
8. Bromo-Noscapine	THR24, THR45, ASN142	853	Complex with Mpro
9. Baloxavir Marboxil	SER46, GLN189,	1000	Complex with Mpro
10. Laninamivir	SER46, ASN142,	5000	Complex with Mpro
11. Ribavirin	SER46, ASN142	2700	Complex with Mpro
12. Coumarin EM01	THR24, SER139, GLU166, THR45,	2000	Complex with Mpro
13. Coumarin EM02	PHE140, ASN142, GLU166, GLN189, HIS163	9	Complex with Mpro
14. Coumarin EM03	LEU141, SER144, GLN189, GLY143,	150	Complex with Mpro
15. Coumarin-EM04	GLN189, HIS41, CYS145, HIS163	150	
16.Hydroxychloroquine	ALA193	1240	Complex with Mpro
17.Tenuifoliside B	THR24, THR25, ASN119, PHE140, GLU166, GLY143	5000	Complex with Mpro

phosphate group of the ligand. These three different types of hydrogen bond interaction largely contributed to the binding energy around −4.08 kcal/mol. The computed toxicity value for the Remdesivir is found to be 1000 respectively (Fig. 1 & Table 2. Molecular docking simulations reveal that remdesivir binds with the Mpro of SARS-CoV-2 and finds support from previous studies [9] (see Fig. 2).

Chloroquine is known to be the most effective anti-malarial drug and anti-ameabiasis, and also has anti-rheumatoid arthritis properties. The docking of Chloroquine with viral protease 6LU7 through GLU166 as the only amino acid residue, with an interaction energy of −2.85 kcal/mol as compared to the interaction energy of −1.53 kcal/mol of Hydroxy-chloroquine through ALA193 (Table 1). The computed toxicity value for Chloroquine was found to be 311 as compared to 1240 for Hydroxy-chloroquine respectively. The computational investigations of antiviral drugs, phytochemicals, and benzylisoquinoline alkaloids with Mpro (Table 1) provide deep insights based on their binding affinities and toxicity values. These new molecules may be considered competent with Remdesivir with regard to their higher binding energies and less toxicity values. The HCQ binds with the binding pocket of the Mpro and finds support from the previous study for 1 μs simulation however, the HCQ does not form any preformed hydrogen bond demonstrated by an in-silico study [53].

The docking of Camostat drug bind through ASN119 and HIS163 amino acids of Mpro having binding energy −4.13 kcal/mol. Also, the

binding energy of Fingolimod with Mpro interacted at amino acids PHE140, ASN142, GLU166, and HIS163 of the same protein and had binding energy of −3.47 kcal/mol. The docking of Galidesivir with Mpro showed affinity to PHE140, LEU141, ASN142, GLN189, and HIS163 amino acids and had binding energy of −3.72 kcal/mol. Moreover, the docking of Favipiravir with Mpro bound with the amino acids THR25, THR45, and SER46 with a binding energy of −3.56 kcal/mol. Some of the antiviral drugs such as Galidesivir, and Remdesivir were granted emergency approval for the use against SARS-CoV-2 but Galidesivir is less effective and does not inhibit SARS-CoV-2 lower than ~100 μM [54].

Noscapine and Bromo-noscapine also exhibited good affinity to the viral protein and interacted at SER46, ASN142, GLN189, THR24, THR45, and ASN142 having corresponding binding energy values of −2.11 kcal/mol and −1.62 kcal/mol respectively. represented the docking of Baloxavir marboxil with viral protease 6LU7, which showed affinity to SER46 and GLN189 amino acids having a binding energy of −1.82 kcal/mol. Docking of Laninamivir with viral protease 6LU7 showed binding with the amino acids SER46, and ASN142 had a binding energy of −5.77 kcal/mol. The molecular docking results with viral protease 6LU7 showed the amino acid residues involved in interaction with ligands.

Ribavirin is bound with Mpro through the amino acids SER46, and ASN142 having a binding energy of −4.57 kcal/mol. Ribavirin is a
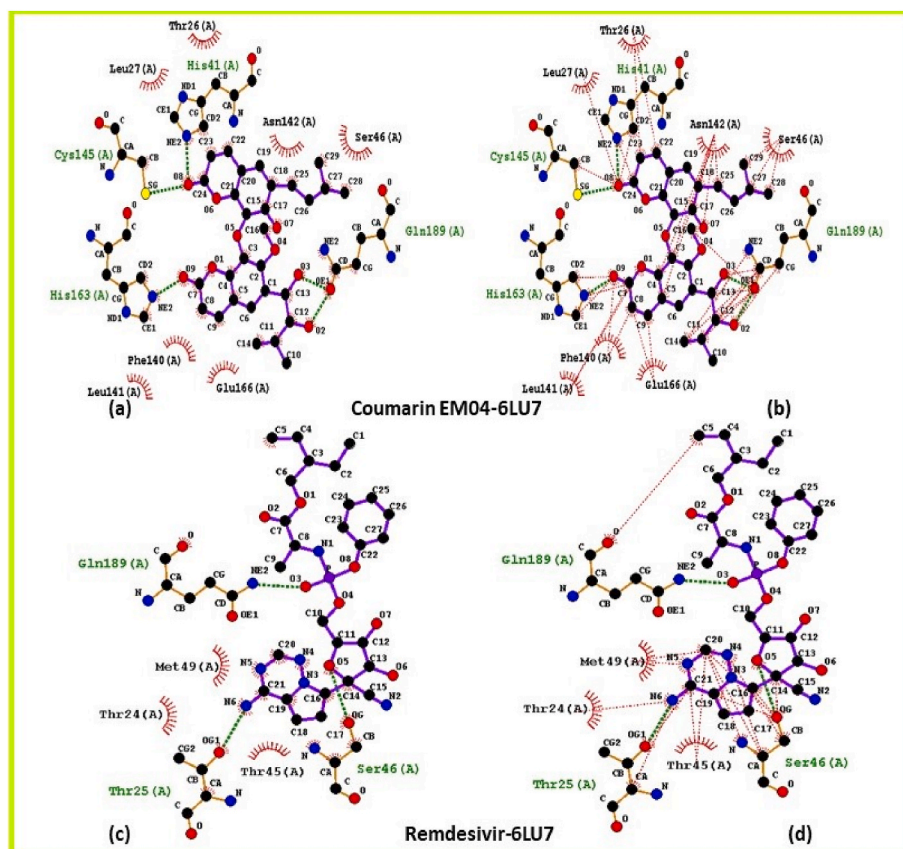
Fig. 3. The 2D visualizations of the Coumarin-EM04 and Remdesivir with the catalytical site of the main viral protease and the interactions exhibited were found with catalytical dyad HIS41 and CYS145 (a) the hydrophobic interactions are represented in red pointed lines (b) and remdesivir fails to achieve the interactions with HIS 41 and CYS 145 subunits of the SARS-CoV-2 (c) hydrogen bonding interactions are represented in green and (d) hydrophobic interactions are represented in red. (For interpretation of the references to color in this figure legend, the reader is referred to the Web version of this article.)
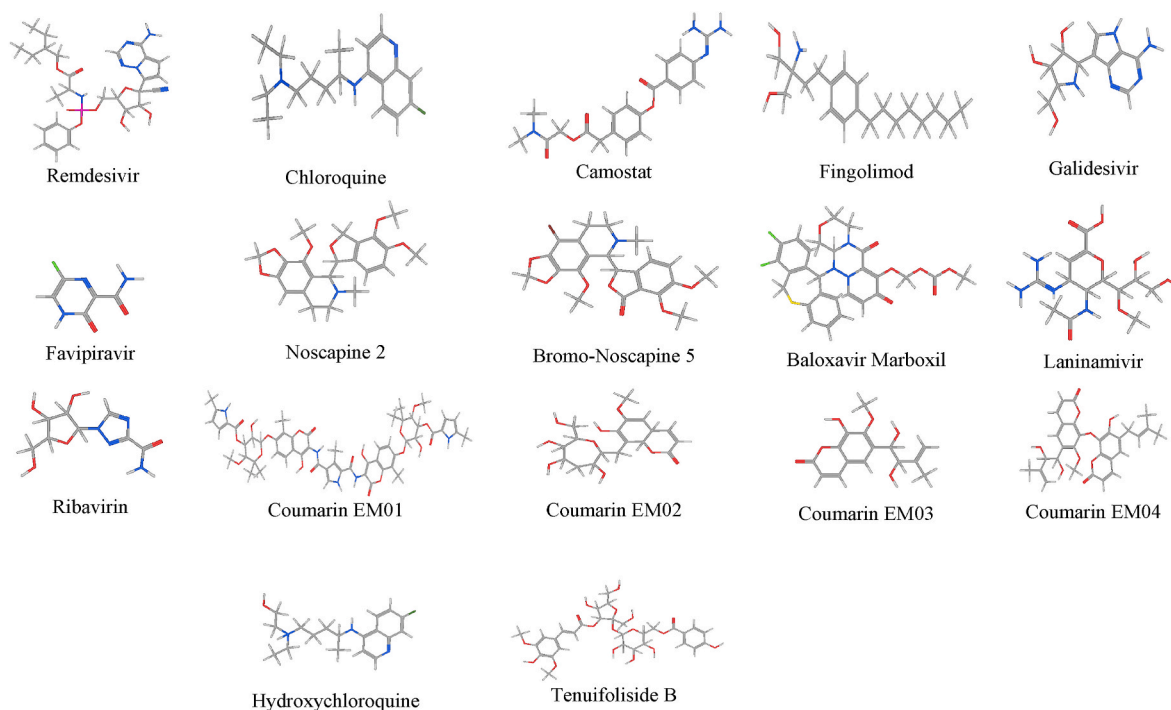

Fig. 4. The 2D structures of the molecules which showed better binding affinity with M^{PRO} main viral protease of SARS-CoV-2.

potential drug candidate to inhibit the Mpro of SARS-CoV-2 [55]. The phenolic moieties of angular Coumarins and alkaloid molecules exploited interactions with the binding site of 6LU7. The flavonoids and polyphenolic phytochemicals showed interactions by OH moieties with dyads Cys164 and His41 [52]. The natural angular Coumarins are anti-HIV modulating agents that inhibit HIV reverse transcriptase at IC_{50} 1.4–1.6 μM [56].
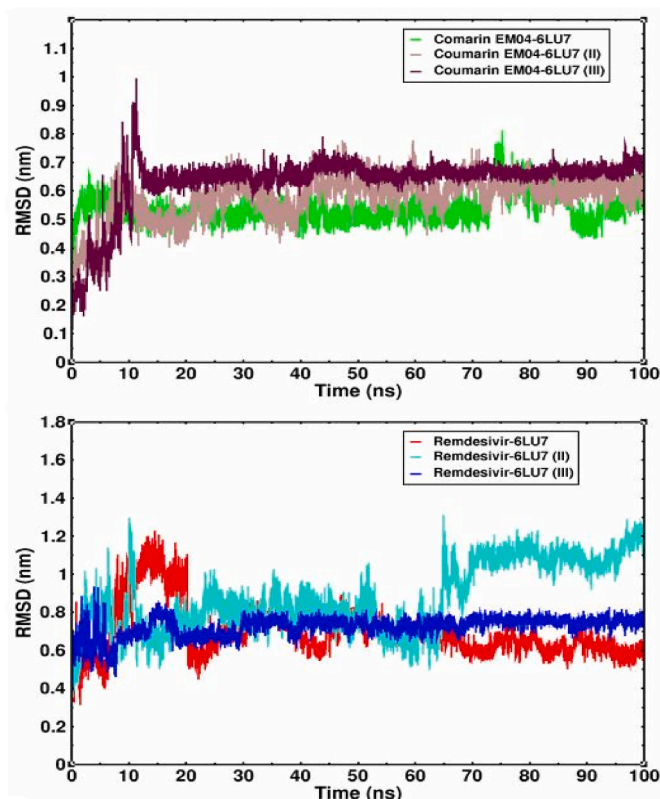
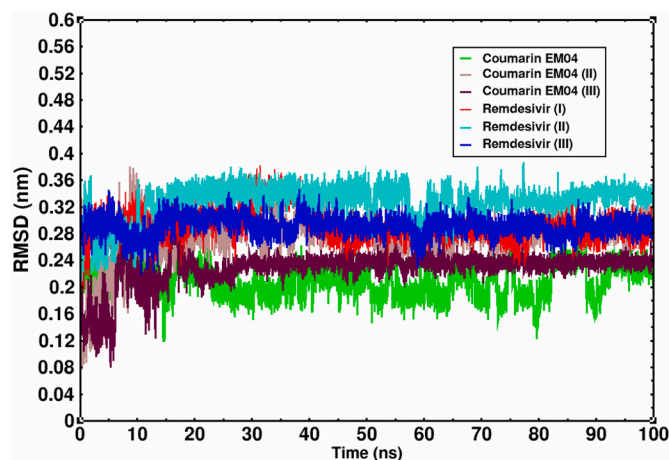The ligand interaction of Coumarin EM01, Coumarin EM02,

Fig. 6. RMSD of ligand when superimposed onto the Ligand for 100ns in an aqueous medium. The color of the first replica was denoted as green, 2nd replica brown, and 3rd replica marron in the case of Coumarin EM04 the color represented as red was assigned for Remdesivir for the first replica, turquoise for 2nd replica and blue for the third replica. (For interpretation of the references to color in this figure legend, the reader is referred to the Web version of this article.)

Fig. 5. RMSD of ligands (Coumarin-EM04 and Remdesivir), when superimposed onto the receptor, 6LU7 viral protein SARS-CoV-2 for 100ns of simulation period in an aqueous medium. The Simulations were done thrice to obtain significant results. The upper plot represented the RMSD of the Coumarin-EM04 with main viral protease whereas the lower plot represented the RMSD of the Remdesivir with SARS-COV-2 protein 6LU7. The color of the first replica was denoted as green, 2nd replica brown, and 3rd replica marron for Coumarin EM04 the color represented as red was assigned for Remdesivir for the first replica, turquoise for 2nd replica, and blue for the third replica. (For interpretation of the references to color in this figure legend, the reader is referred to the Web version of this article.)

Coumarin EM03, and Coumarin-EM04 was obtained. Coumarin EM01 interacted through THR24, SER139, GLU166, and THR45 having with highest binding energy value, −5.14 kcal/mol as compared to the other three. The computed binding interaction energy of Coumarin EM02 (PHE140, ASN142, GLU166, GLN189, HIS163), Coumarin EM03 (LEU141, SER144, GLN189, GLY143), and Coumarin-EM04 (GLN189, HIS41, CYS145, HIS163) were found to be −4.48 kcal/mol, −4.36 kcal/mol, and −4.51 kcal/mol respectively (Figs. 1 and 3). Based on their computed toxicity value (Table 2), these coumarins molecules are very promising for synthesis and their usage as competitive to Remdesivir as an antiviral drug against SARS-CoV-2.

Tenuifoliside B exhibited a higher binding affinity value of −6.25 kcal/mol with 6LU7 interacting through the amino acid residues: THR24, THR25, ASN119, PHE140, GLU166, and GLY143. Tenuifoliside B interacted with the binding pocket of 6LU7 through OH groups of amino acids based on six different hydrogen bond interactions but no interactions were observed with the catalytical dyad.

Among these documented 17 different molecules (Fig. 4), Coumarin-EM04 was found to be promising and effective as compared to Remdesivir based on their high binding affinities (Table 1) and, low toxicity values (Table 2). Based on the molecular docking studies on seventeen different molecules, Tenuifoliside B exhibited a higher binding affinity value of −6.25 kcal/mol with 6LU7 interacting through the amino acid residues: THR24, THR25, ASN119, PHE140, GLU166, GLY143 with OH

groups of amino acids on six different hydrogen bond interactions but no interactions were observed with the catalytical dyad and Coumarin-EM04 showed binding affinity of −4.51 kcal/mol with main viral protease and interactions were observed with the catalytical dyad HIS41 and CYS145 amino acids.

For further in-silico investigations, we have taken remdesivir as a control because of its dual inhibition potency against SARS-COV-2. Remdesivir inhibits the RNA-dependent RNA polymerase of SARS-CoV-2 also remdesivir is a target of Mpro thus remdesivir has the ability to bind with dual targets RdRp and Mpro of SARS-CoV-2 [57].

3.2. Toxicity analysis

Protox II web server is used to predict the toxicity of molecules under five different classes of toxicities, Class I: fatal if swallowed (LD50 ≤ 5) Class II: fatal if swallowed (5 < LD50 ≤ 50) Class III: toxic if swallowed (50 < LD50 ≤ 300) Class IV: harmful if swallowed (300 < LD50 ≤ 2000) Class V: may be harmful if swallowed (2000 < LD50 ≤ 5000 Class VI: non-toxic (LD50 > 5000). The LD_{50} value of Remdesivir is 1000 mg/kg and Coumarin-EM04 is 150 mg/kg rest predicted values of all molecules are mentioned in Table 2. However, the toxicity model shows Hydroxychloroquine, chloroquine, and coumarins come under toxicity classes III & IV [22,52,56]. These investigations demonstrated Coumarin-EM04 could be a more effective agent against the Mpro of COVID-19.

3.3. Molecular dynamics simulations

The findings for the Coumarin-EM04 interaction with 6LU7 further encourage us to carry out a Molecular Dynamics Simulation study thrice to achieve significant results. Fig. 4 represents the RMSD of Coumarin-EM04 with SARS-CoV-2. It was observed that the RMSD of coumarin EM04 remains between 0.5 nm and 0.65 nm until the completion of the simulation time period and linear RMSD trajectories were observed in each replica. This means that the Coumarin EM04 molecule showed robust bindings and remains stable in the binding site of the template protein (6LU7) main viral protease of COVID-19. The average RMSD reflected by Remdesivir with M^PRO protein was found to be 0.6–0.8 nm till 65 ns of simulations thereafter slight differences were observed after 65 ns and RMSD was found to be 0.8–0.9 nm. The overall findings showed that Remdesivir showed parallel stability like Coumarin-EM04 against the main viral protease of the SARS-CoV-2 (Fig. 5).
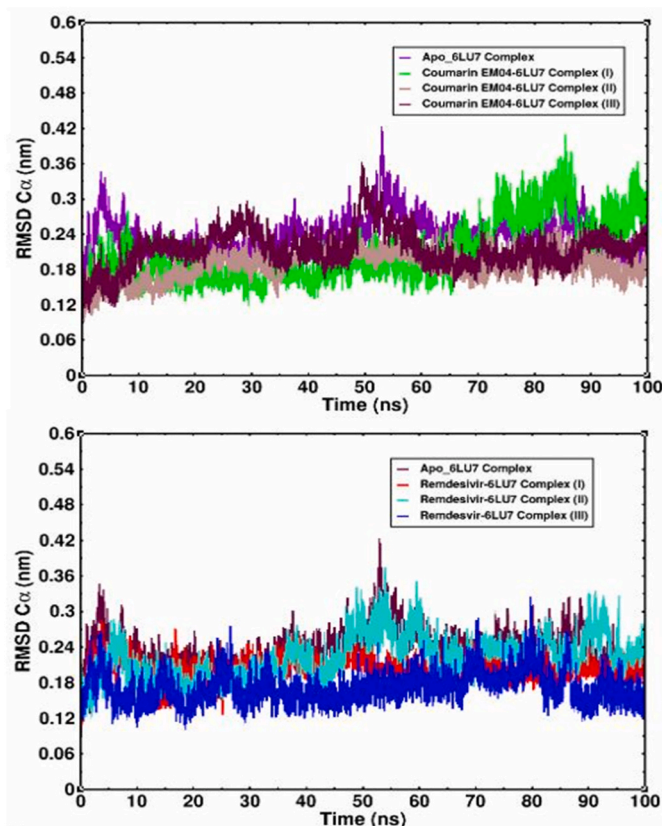
Fig. 7. RMSD of 6LU7 backbone Cα indicates the stability of the simulated complexes of viral protein bound with Coumarin-EM04 and Remdesivir including Apo complex for 100ns of simulation period in the aqueous medium. The complexes are represented in Apo violet, Coumarin-EM04 green, brown, and maroon, and for Remdesivir the trajectories are represented as red, turquoise, and blue. The upper plot represents Coumarin-EM04 bound with 6LU7 including Apo trajectory was colored violet. The lower plot represents the trajectories of Remdesivir bound with 6lu7 and the Apo complex backbone Cα trajectory is represented in marron. (For interpretation of the references to color in this figure legend, the reader is referred to the Web version of this article.)

The linear trajectory reflected from MDS envisages that Coumarin-EM04 may also have SARS-COV-2 inhibition potency and may serve as a better inhibitor against Mpro. The stability of the Coumarin EM04 with 6LU7 was observed generally after 10 ns of MDS whereas the higher RMSD was observed in the 2nd replica after 65 ns of MDS.

The average RMSD of the ligand Coumarin EM04, during the simulation period, was found between 0.2 nm–0.24 nm whereas the average RMSD displayed by the Remdesivir was found to be 0.28–0.32 nm throughout the simulation period which reveal the stability of ligands were observed upon the superimposed on respective ligand during molecular dynamics simulations (Fig. 6). The average RMSD of backbone Cα of the 6LU7 was investigated and found the trajectories of Coumarin-EM04 bound 6LU7 remain within the range of 0.12 nm–0.18 nm for 70 ns of the simulation period but after 70 ns a slight increase of Cα was found and the RMSD lay between 0.2 and 0.4 nm (Fig. 7). Also, the average mean RMSD of the Cα backbone of 6LU7 bound with remdesivir was computed and the values lay between 0.12 and 0.19 nm throughout the simulation period. The Apo complex of 6LU7 without ligand was computed to determine the RMSD of backbone Cα. The RMSD backbone Cα of Apo complex was found between 0.2 and 0.3 for the first 50 ns after when simulation reaches the RMSD of backbone Cα increases and RMSD values are within 0.25–0.4 nm then again RMSD of backbone Cα decreases and values were observed between 0.22 and 0.3 nm throughout the simulation period. This indicates the stability of each
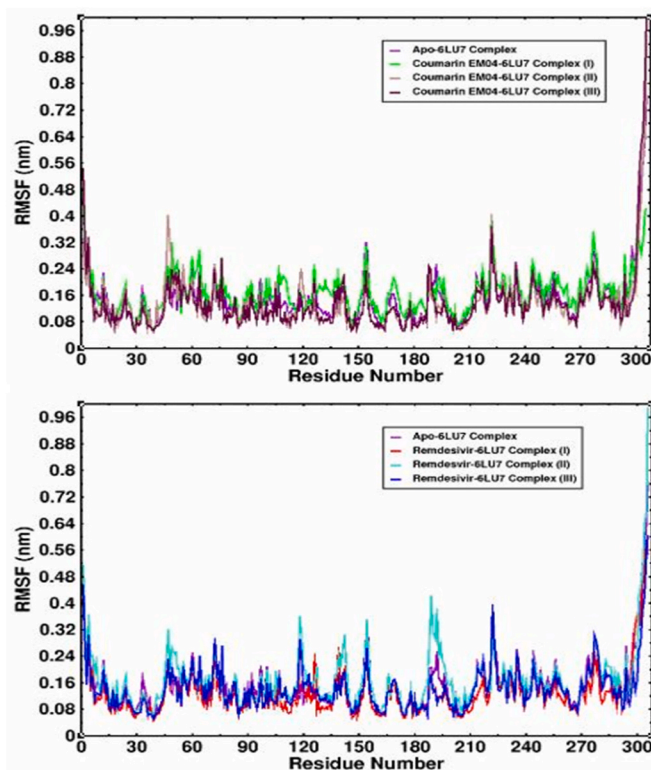

Fig. 8. RMSF of amino acid residues of 6LU7viral protein bound with Coumarin-EM04, remdesivir, and Apo complex without ligand for 100ns of Simulation Period in an aqueous medium. The trajectories are represented by different colors and given in the legend box of the plot. Similarly, the fluctuations of amino acids of 6LU7 bound with Coumarin-EM04 was represented in the upper plot, and colors were given as violet for Apo complex green, brown, and marron were assigned for replica 1st, 2nd, and 3rd whereas the lower plot of the RMSF represents Remdesivir bound with the 6LU7 and colors are indicated as violet for Apo, red, turquoise and blue were assigned for 1st, 2nd, and 3rd replica. (For interpretation of the references to color in this figure legend, the reader is referred to the Web version of this article.)

complex Coumarin-EM04 and Remdesivir bound 6LU7 including the Apo complex of the main viral protease SARS-CoV-2 protein and the obtained data was found within acceptable limits. The root mean square fluctuations (RMSF) of 6LU7 viral protein bound with Coumarin-EM04, Remdesivir and alone Apo complexes were investigated and found that all amino acids present in the viral protein show low RMSF, higher fluctuations were found only in the N-terminal region of the protein in each simulation. The catalytic dyad amino acids showed average fluctuations of 0.05–0.14 nm of 6LU7 bound Coumarin-EM04 calculated from the triplicates also the catalytic dyad displayed lower fluctuations in the Apo complex but at the N terminal showed higher fluctuations as compared to the other two complexes Fig. 8. The radius of gyration (Rg) was also calculated and the Rg trajectory (Fig. 9) reflects the compactness of the protein when simulated with the Coumarin-EM04 in triplicates. The average Rg values were found between the 2.22 nm–2.24 nm range in both complexes bound with ligands (Coumarin-EM04 and remdesivir). In the case of the Apo complex, the average Rg values were found between 2.22 and 2.24 nm for the first 50 ns but then increase ranging between 2.24 and 2.28 nm. The lower Rg value determines the higher compactness of the protein [58]. The Apo protein showed less compactness whereas the ligand-bound complexes showed more compactness than Apo this suggested that the conformational changes occur by the ligand bindings and make the protein more stable.

Solvent-accessible surface area (SASA) is known to be a thrust force on protein folding. The atoms present in a protein correlate with
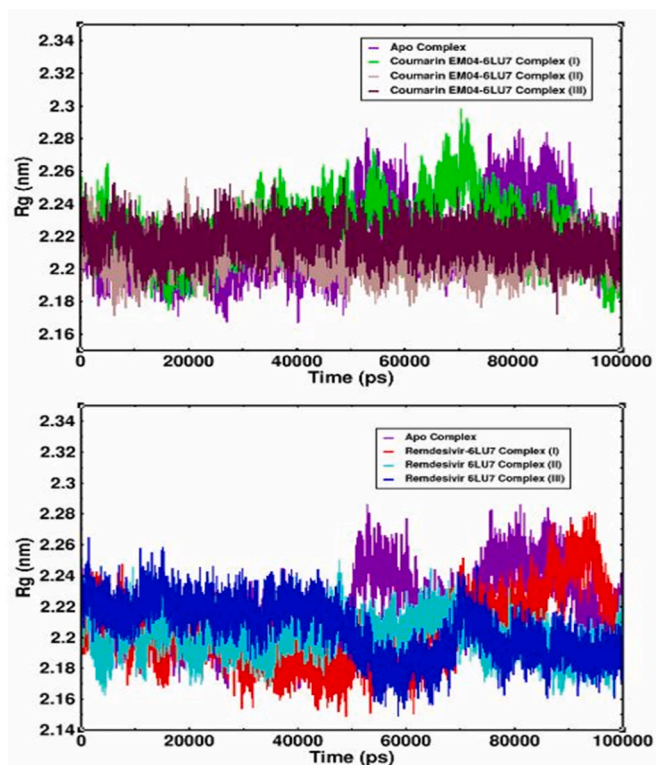
Fig. 9. The radius of gyration of the simulated complexes bound with Coumarin-EM04 and Remdesivir reflected compactness more than that of the Apo complex, computed for 100 ns in triplicates in an aqueous medium. The upper plot represented the RMSD of the Coumarin-EM04 with main viral protease whereas the lower plot represented the RMSD of the Remdesivir with SARS-COV-2 protein 6LU7. The color of the first replica was denoted as green, 2nd replica brown, and 3rd replica marron for Coumarin EM04 the color represented as red was assigned for Remdesivir for the first replica, turquoise for 2nd replica, and blue for the third replica. The trajectory of the Apo complex was colored in violet. (For interpretation of the references to color in this figure legend, the reader is referred to the Web version of this article.)
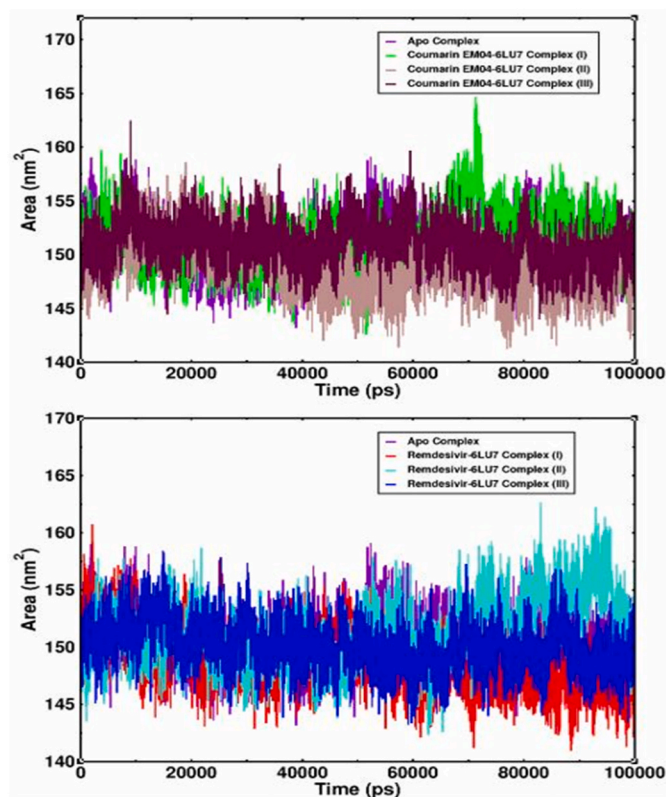

Fig. 10. The protein folding was determined by computing SASA of the simulated complexes bound with Coumarin-EM04 and Remdesivir reflected compactness more than that of Apo complex, computed for 100 ns in triplicates in an aqueous medium. The upper plot represents the SASA of the Coumarin-EM04 with main viral protease whereas the lower plot represented the SASA of the Remdesivir with SARS-COV-2 protein 6LU7. The color of the first replica was denoted as green, 2nd replica brown, and 3rd replica marron for Coumarin EM04 the color red was assigned for Remdesivir for the first replica, turquoise for 2nd replica, and blue for the third replica. The trajectory of the Apo complex was colored violet. The protein folding was found comparable to that of the Apo complex. (For interpretation of the references to color in this figure legend, the reader is referred to the Web version of this article.)

the hydrophobicity and protein folding process. The computed SASA values were depicted in Fig. 9. It has been observed that for the first 100 ns, it lays within 148 nm–160 nm and then the value slightly increases at 70 ns and then decreases observed in coumarin-EM04 bound complex but remdesivir bound 6LU7 main viral protease showed decreasing trend among SASA values from initial frame till end of the simulations. The SASA calculations reflect the average folding of the 6LU7 protein bound with ligands than Apo complex during 100ns of the simulation period Fig. 10.

The number of hydrogen bonds formed by Coumarin-EM04 with the main viral protease was found to be 6 for the 1st and 2nd replica and for the 3rd replica the hydrogen bond contacts were found to be 3 (Fig. 11). The Remdesivir showed hydrogen bond contacts 6 for 1st replica, 2 hydrogen bond contacts in 2nd replica and for 3rd replica the hydrogen bond contacts were found to be 3. Also, the solvent contacts displayed by the Coumarin-EM04 and Remdesivir was found to be 32 and 42 during the simulation period.

3.4. Average bond distance during molecular dynamics simulations

The Hydrogen bond distances were analyzed for all the interactions obtained in molecular docking simulations. During molecular dynamic simulations, it has been noted that the interactions are within the binding site as well as with the catalytic dyad for 100 ns (Fig. 12). Five bonding interactions were exhibited by the Coumarin-EM04 with the M^{PRO} main viral proteases of the SARS-CoV-2 and the amino acids that

participated with the bindings are HIS41, CYs145, HIS163, and GLN189 respectively. The Remdesivir displayed bonding interactions via amino acids THR25, SER46, and GLN189. The hydrogen bond distance of the interacted ligand moieties with the Mpro was computed for 100ns of simulation length which provides more insights into the ligand bindings with the protein. The average hydrogen bond distance of all the binding interactions and standard deviations were computed and are represented in Table 3.

3.5. Principal component analysis and Gibbs energy landscape investigations

The flexibility of a protein is commonly determined using essential dynamics [47,48]. The PCA was used to analyze the protein movements and variations of the simulated main viral protease M^{PRO} bound with Coumarin-EM04 and Remdisivir by using backbone Cα trajectory data. The eigenvalues and eigenvectors were calculated, using gmx the *gmx covar,* and *angien* modules, and the principal components were determined (PC1 & PC2). The difference between the three sampled systems of main viral protease M^{PRO} bound with Coumarin-EM04 and Remdisivir and Apo Complex was shown by the PCA scatter plot created from Cα. (Fig. 13).

This essential dynamic provides insights into the structural conformity of the complexes. Further, the Gibbs energy landscape was done to
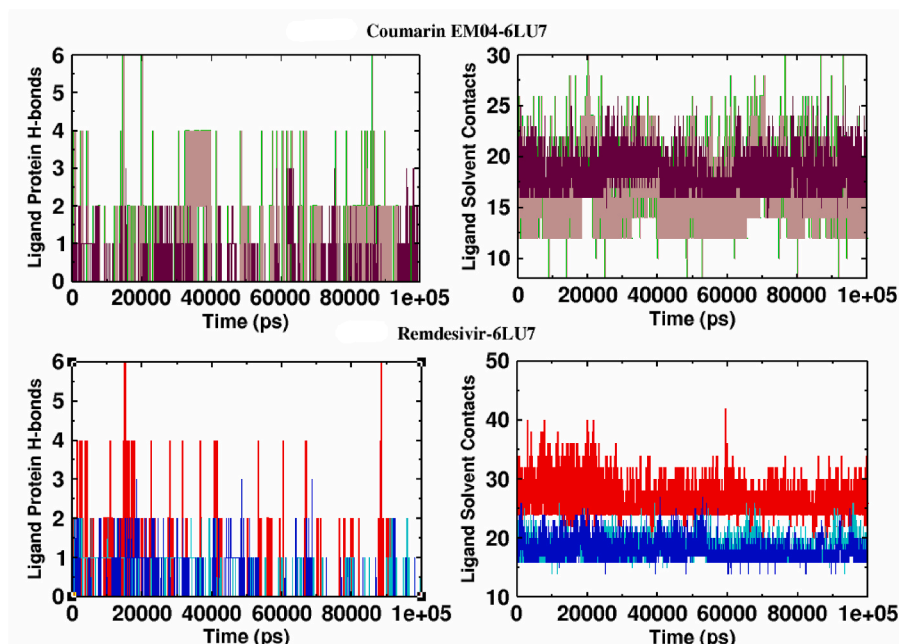
Fig. 11. The Ligands exhibited hydrogen bond contacts with M^PRO of SARS-CoV-2 (Left) also the ligands displayed the solvent contacts embedded in the simulated box are represented in right.

determine the meta-energy stable states of the complexes (Fig. 14). The Gibbs energy landscape was computed for three sampled systems, Coumarin-EM04 and Remdisivir bound main viral protease M^PRO and Apo complex. The red color indicated the maximal stable conformations state whereas the blue color denoted the minimal conformational stable energy of the sampled system. The average Gibbs energy landscape of Remdisivir bound main viral protease Mpro was found to be 13.46 kJ/mol, and Coumarin-EM04 bound 6LU7 showed 12.83 kJ/mol (Fig. 13). The Apo complex displayed Gibbs energy landscape values of 13 kJ/mol. The Coumarin-EM04 bound M^PRO achieved the highest metastable conformations than Remdisivir bound main viral protease SARS-COV-2 and Apo Complex.

4. Structural conformational changes in complexes during molecular dynamics simulations

Molecular dynamics simulations are an essential tool to observe the conformation changes of ligands and their orientations during the dynamics run, probably to identify whether the ligand is in the binding site or out of the binding during simulations. The triplicate MDS was performed to achieve significant results and a deep understanding of ligand orientations and conformational changes in ligands during simulations. The protein-ligand complexes were dumped after completion of the equilibrium run NVT and NPT 100 ps steps of each run. Simultaneously after a production run of 100 ns complexes (protein & ligand) were dumped at 25 ns, 50 ns, 75 ns, and 100 ns. The protein conformations were monitored at different time scales during MD simulations of complexes bound with Coumarin-EM04 and Remdesivir including Apo complex (without ligand). The Apo complex shows different conformations at different time scales however at 100 ns conformations it was found the homodimer interface consists of 28 amino acids communicated with domain 1 composed of 189 amino acids showing structural changes this demonstrates that without ligand in the binding site, structural conformational changes occurred at the end of simulations. The main viral protease of SARS-CoV-2 bound with Coumarin-EM04 showed conformational changes at 25 ns and 50 ns of time scale but at 75 ns and 100 ns, it was observed the complex achieved a secondary structure close to the native structure. The effects on the structure during simulations bound with remdesivir showed significant conformations in

replicas (I&II), whereas the third replica showed a secondary structure at 100 ns close to the native structure. This study demonstrates Coumarin EM-04 does not show any effect upon the structure during a long simulation run but in the case of remdesivir effects in the structure were observed in the main viral protease.

The conformational changes of Coumarin-EM04 bound with Mpro were studied and in the first replica, it was observed at 75 ns of simulations, conformational changes in ligand occurred which is depicted as the ligand traveled towards the surface of the main viral protease protein Mpro then after Coumarin-EM04 retains its orientations as analyzed at 200 ps, 25 ns, and 50 ns. Also, in the 2nd and 3rd replicas of the simulations of Coumarin-EM04 bound Mpro complexes, it was found that the orientations achieved by ligand at 200 ps were found similar at the end of the simulations.

The conformational changes observed in remdesivir bound Mpro were also monitored for 100 ns in three different simulation runs. It was observed the conformations and orientations of the Remdesivir were similar in each complex at different ns of the time scale but in the case of the 2nd replica, the conformational state of the ligand at 25 ns rotates at 180 °C and remains in the same conformations state till 50 ns thereafter 90 °C rotations occur in remdesivir at 75 ns then the orientations remain similar till the end of the simulation in the binding site These conformations in orientations of remdesivir in the binding site showed large RMSD values and the ligand was found at the surface of the 6LU7. The conformational changes in the ligands among 6 simulation runs showed good agreement with the RMSD analysis Fig. 5.

The Definition Secondary Structure of Protein (dssp) module of gromacs was chosen to determine the structural changes of the Mpro upon the bindings of coumarin-EM04 and remdesivir of SARS-CoV-2.

The Mpro protein of SARS-CoV-2 has 150 residues classified as hydrophobic and 156 are hydrophilic. The Mpro complexed with coumarin-EM04 showed transitions between the α-helix and turns represented in blue and yellow color (Fig. 15). It was also observed from the secondary structure reaches approximately the native structure at the end of the simulations. However, the Mpro complexed with the remdesivir also showed transitions between the α-helix and turns represented in the secondary structure (Fig. 16). Also, it was observed that the transition occurs α-helix and bends represented in blue and dark green. The Definition Secondary Structure of Protein (dssp) analysis
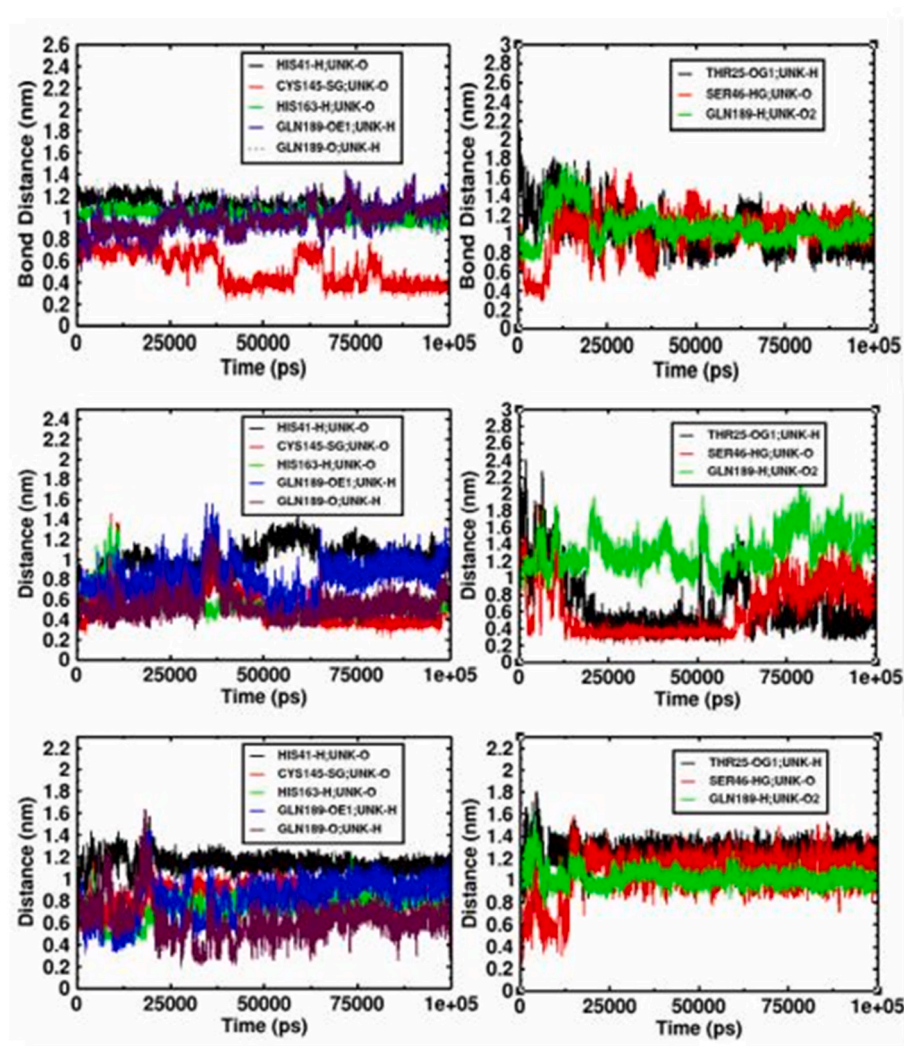
Fig. 12. Hydrogen Bond Distances of interaction site of amino acids: 41, 145, 163, and 189 of 6LU7 viral protein with Coumarin-EM04 and amino acids 25, 46, and 189 of 6LU7 viral protein with remdesivir for 100ns of Simulation Period in an aqueous medium.

Table 3

The average distance and standard deviation of all Hydrogen Bond distances displayed by the Coumarin EM04 and Remdesivir.

S. No.	Ligand Interaction	Average Distance (nm)	Standard Deviation (nm)
Coumarin-EM04-6LU7			
1	Amino acid 41:H, LIG:O	1.10918	0.06410
2	Amino acid 145: SG, LIG:O	0.52050	0.15142
3	Amino acid 163: H, LIG:O	1.01977	0.04868
4	Amino acid 189: OE1, LIG:H	0.98166	0.12203
5	Amino acid 189:O, LIG:H	0.98022	0.12176
Remidesivir-6LU7			
1	Amino acid 25:OG1, LIG:H	1.05277	0.22736
2	Amino acid 46:HG, LIG:O	1.02327	0.22183
3	Amino acid 189:H, LIG:O2	1.06812	0.16243

demonstrates that Coumarin-EM04 complexed with the Mpro remains stable whereas remdesivir bound Mpro showed transitions between α-helix and turns and bends throughout the simulation time.

4.1. Free energy calculations through the MMPBSA method

The molecular mechanics poisson Boltzmann's surface area (MMPBSA) method using g_mmpbsa module of the Gromacs 5.1.1. The free energy binding of Coumarin-EM04 and Remdesivir was calculated from the middle 60–70 ns frames of reflected trajectories obtained during molecular dynamics simulations. The needed MmPbSaStat.py file was used to calculate the binding affinities of ligands with the respective protein and bootstrap analysis was used to determine the average free energy bindings. The free binding energy is a sum of changes in electrostatic energy, van der Waals energy, SASA energy, and polar solvation energy. The average binding free energy calculated from three replicas and the exhibited ΔG of Coumarin-EM04 was found to be −187.471 ± 2.230 kJ/mol and Remdesivir displayed −171.926 ± 2.237 kJ/mol respectively (Table 4). The present findings reveled that the ΔG binding of Coumarin-EM04 exhibited with the 6LU7 is higher than the remdesivir.

4.2. Net free energy contributions by each amino acid in simulated complexes

Further, the net contributions of free binding energy by each amino acid residue during simulations were calculated by using the MmPbSa-Decomp.py code. The favorable energy contributions by residues of the
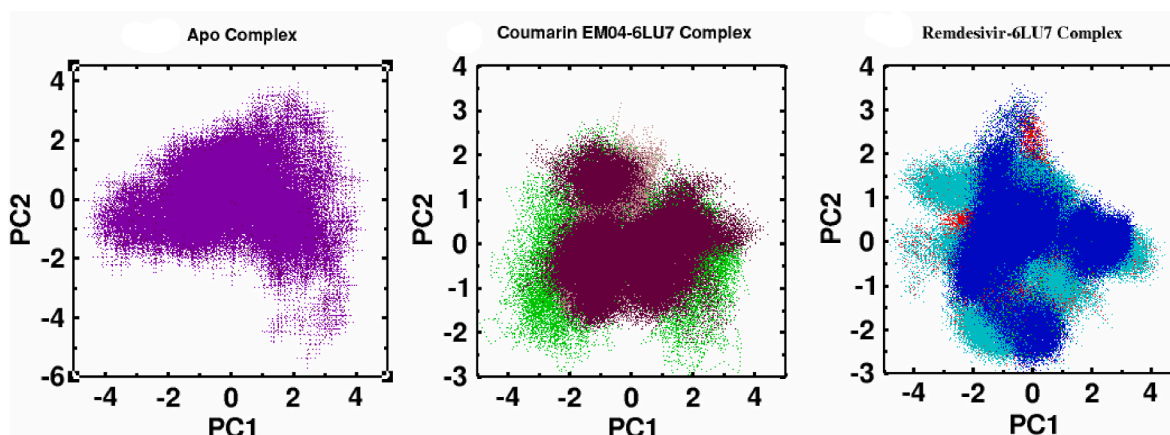
Fig. 13. The flexibility and protein motions are determined for 100 ns of time scale Apo complex and Coumarin-EM04 bound M^{PRO} showed comparable motions whereas remdesivir bound M^{PRO} more flexibility and motions calculated by principal component analysis.
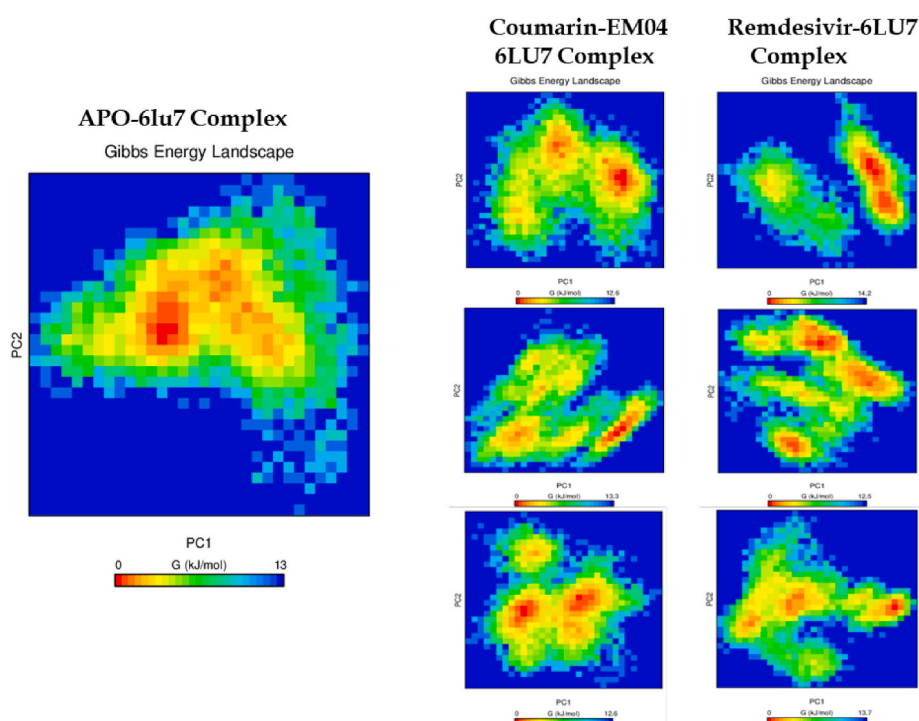

Fig. 14. The Gibbs energy landscape was done using the g_sham module of the gromacs. Each complex differs in metastable conformations. The lowest stable conformational stability was shown by the Coumarin-EM04 bound main viral protease Mpro of the SARS-CoV-2.

main viral protease M^{PRO} bound Coumarin-EM04 were found among amino acid residues LEU27 = −2.400, ARG40 = - 2.4744, HIS41 = −3.644, ASP48 = −3.2814, MET49–1.2227, ARG105 = −2.3729, GLY143 = −2.6880, SER144 = −3.7765, CYS145 = −6.1777, ASP187 = −4.5738, MET165 = −12.0814 and GLN189 = −13.4798 kJ/mol and net free energy decomposition contributed by ligand is −113.0398 kJ/mol. The Remdesivir bound main viral protease M^{PRO} showed net higher decomposition energy exhibited by amino acid THR24 = −9.0242, THR25 = −13.5815, THR26 = −12.1082, HIS41 = −2.4359, ASP48 = −3.4855, MET49–3.0323, CYS145 = −1.3845, and MET165 = - 2.4972 kJ/mol and net free energy decomposition contributed by ligand is −79.9180 kJ/mol (Fig. 17). The study demonstrated that the ΔG binding of the Coumarin-EM04 is higher than that of the ΔG binding of Remdesivir computed with the main viral protease of SARS-CoV-2. Both complexes Coumarin-EM04 and remdesivir bound main viral protease showed catalytical dyad HIS41 and CYS145 are involved in the free

energy contributions but Coumarin-EM04 bound main viral protease displayed higher negative free energy contributions by the catalytical dyad amino acids HIS41 and CYS145 than remdesivir bound main viral protease which implies Coumarin-EM04 perfectly accommodates in the binding site of main viral protease.

Several studies predicted the ΔG displayed by the remdesivir is −36.75 kcal/mol against Nucleocapsid SARS-CoV-2(B.1.351) and −36.00 kcal/mol Nucleocapsid SARS-CoV-2Omicron (B.1.1.529) which is equal to ΔGbind displayed by remdesivir with the M^{PRO}. Other phytochemicals such as 4,8-dihydroxy sesamin, arboreal, favipiravir, and hydroxychloroquine were studied by Jency Roshni et al., 2022 [59] against the Nucleocapsid SARS-CoV-2(B.1.351) and Nucleocapsid SARS-CoV-2Omicron (B.1.1.529). Also, phytochemical withanolide R and 2,3-Dihydrowithaferin A displayed ΔG binding with main viral protease were −144.96 kJ/mol and −87.60 kJ/mol respectively studied by Ref. [60]. Moreover, the phytochemicals present in the black tea
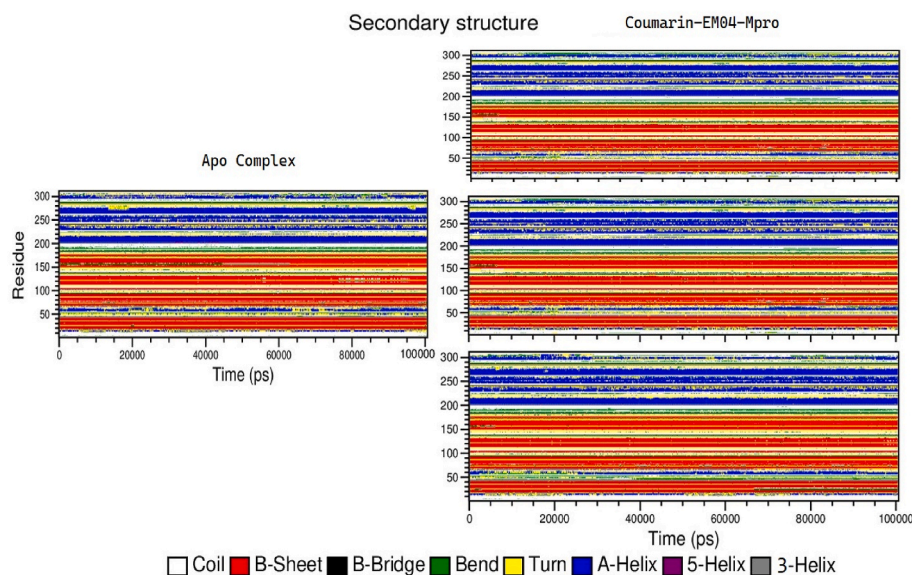
Fig. 15. Definition Secondary Structure of Protein (DSSP) analysis of Mpro complexed with the Coumarin-EM04 and remdesivir at different time periods was visualized using VMD. In the case of Coumarin bound Mpro, the transition from α-Helix to the turns was observed at 5–25 ns of time periods and Apo complex shows transition at 25, 70, and 75 ns of the time period.
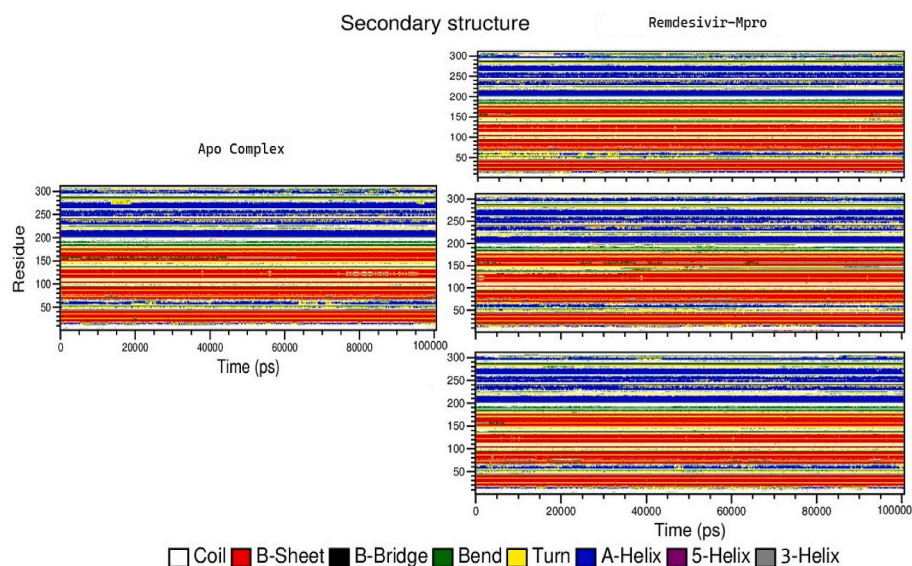

Fig. 16. Definition Secondary Structure of Protein (DSSP) analysis. In the case of Remdesivir bound Mpro, the transition from α-Helix to the turns was observed throughout the simulation period.

Table 4
The free energy binding of Coumarin-EM04 and remdesivir against the main viral protease of SARS-CoV-2.

Complex	$\Delta E_{binding}$(kJ/mol)	$\Delta E_{Electrostatic}$ (kJ/mol)	$\Delta E_{Polar\ solvation}$ (kJ/mol)	$\Delta E_{vander\ Wall}$ (kJ/mol)	SASA (kJ/mol)
Coumarin-EM04(I)	−185.708 ± 2.616	−107.726 ± 2.801	176.706 ± 1.157	−231.368 ± 1.256	−23.309 ± 0.108
Coumarin-EM04(II)	−189.190 ± 2.054	−110.542 ± 2.075	178.055 ± 0.885	−233.302 ± 0.943	−23.370 ± 0.885
Coumarin-EM04(III)	−187.516 ± 2.022	−108.325 ± 2.107	177.076 ± 0.957	−232.280 ± 1.421	−23.329 ± 0.902
Remdesivir(I)	−153.526 ± 3.316	−126.725 ± 4.395	109.602 ± 2.115	−129.209 ± 2.757	−17.309 ± 0.304
Remdesivir(II)	−182.068 ± 1.575	−104.231 ± 1.185	124.191 ± 1.260	−1821.603 ± 1.443	−20.437 ± 0.112
Remdesivir(III)	−180.186 ± 1.820	−173.209 ± 2.714	138.300 ± 1.756	−129.696 ± 0.983	−15.5.6 ± 0.108

theaflavin 3,3′-di-gallate (TF3), Procyanidin B2, and theaflavin 3-gallate were screened against multiple targets of the SARS-CoV-2 showed binding affinity −93.59, −139.78 and −96.88 kJ/mol [61]. Even though the Limonoids and triterpenoids such as molecules ID CHEMBL502955, CHEMBL2335028, and CHEMBL4215430 were

identified as potent inhibitors of SARS-CoV-2 M^{PRO} exhibited ΔG binding −163.72, −136.83, and −122.31 kJ/mol [45]. Present in-silico investigations decipher that previously studied molecules are less effective against SARS-CoV-2 than Coumarin-EM04 and the bindings exploited by the Coumarin-EM04 with the main viral protease involving HIS41 and
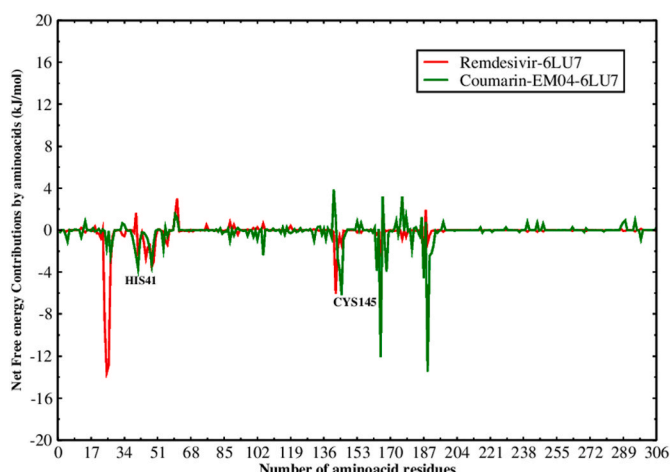
Fig. 17. Net free energy contribution by the 6LU7 bound with Coumarin-EM04 and Remdesivir is represented in green and red plots also catalytic dyad amino acid names are mentioned in the graph. (For interpretation of the references to color in this figure legend, the reader is referred to the Web version of this article.)

CYS145. The Coumarin-EM04 remain stable in the catalytical site of the Mpro for a long-range simulation run and was computed thrice. Also, HIS41 and CYS145 take part in net free energy decompositions which validate the molecular docking simulations. Also, the free binding energy of Coumarin-EM04 was found to be -187.471 ± 2.230 kJ/mol which is higher than remdesivir -171.926 ± 2.237 kJ/mol against main viral protease Mpro. These computational investigations resulted in Coumarin EM04 may inhibit the duplication of SARS-CoV-2 main viral protease by blocking the catalytical site and thus stop the furin cleavage.

Generally, computational models have their own limitations that can be used for preliminary investigations and formulate simulation-based theories only. So, the modeled hypothesis in a closed environment needs to be validated and is an essential part of the research. The present study focused on the interplay of the small molecules with the catalytical site of the main viral protease (Mpro) to observe their stability and their effects on the Mpro protein of SARS-CoV-2. This study needs to be exaggerated to in-vitro and in-vivo models.

5. Conclusion

The molecular docking strategy along with the molecular dynamics simulations study has been adapted to predict the comparative bindings and interactions of 17 different molecules out of 72 derivatives of Coumarins, 5 molecules of Noscapine analogs, and 22 reported antiviral drug molecules (a total of 99 molecules). The present investigations reveal that antiviral drugs like Coumarin-EM04 were found to be promising and effective as compared to Remdesivir based on their high binding affinities with 6LU7, stability, and binding-free energy. Coumarin-EM04 exhibits a higher binding affinity value of -4.51 kcal/mol with 6LU7 interacting through the amino acid residues HIS41, CYS145, SER165, and GLN189 based on five different hydrogen bond interactions as compared to the other coumarin molecules, Noscapine derivatives, and antiviral drugs. Further, the Molecular Dynamics Simulation study also reveals that Coumarin-EM04 remains stable in the binding site of 6LU7 for 100ns of simulations based on the RMSD of Ligand movement, Ligand Conformations, RMSD of backbone Cα of viral protein, Radius of gyration, Solvent accessible surface area, and Hydrogen bond distances. The free binding energy was found better in the case of Coumarin-EM04–187.471 $\pm$ 2.230 kJ/mol than remdesivir -171.926 ± 2.237 kJ/mol against main viral protease Mpro of SARS-CoV-2. The present investigation is also proposed to be very promising towards synthesis and their usage as a competent antiviral drug against

COVID-19 Mpro, based on the computed toxicity value. Moreover, *in vivo* and *in vitro* studies in the future may validate the present computational model investigations.

Contributions

SAM Contributes the Software, modeling, Simulation and Free binding energy calculations. SAM, RKM and BN contributes to manuscript preparations, data curation, data analysis and interpretations. SAM and BN supervised the work.

Declaration of competing interest

All authors declare no conflict of interest.

Data availability

Data will be made available on request.

References

[1] http://www.emro.who.int/health-topics/corona-virus/transmission-of-covid-19-by asymptomatic-cases.html.
[2] Nan Jing, Jin Yu-Bo, Myo Yunjung, Zhang Ge, Hypoxia in acute cardiac injury of coronavirus disease 2019: lesson learned from pathological studies, J Geriatr Cardiol 4 (2020) 221–223.
[3] L.L. Poon, M. Peiris, Emergence of a novel human coronavirus threatening human health, Nat. Med. 3 (2020) 317–319.
[4] A.C. Walls, Y.J. Park, M.A. Tortorici, A. Wall, A.T. McGuire, D. Veesler, Structure, function, and antigenicity of the SARS-CoV-2 spike glycoprotein, Cell (2020) *Cell*, *181*(2), 281-292.
[5] A. Hasan, B.A. Paray, A. Hussain, F.A. Qadir, F. Attar, F.M. Aziz, K. Shah pasand, A review on the cleavage priming of the spike protein on coronavirus by angiotensin-converting enzyme-2 and furin, J. Biomol. Struct. Dyn. 1–9 (2020).
[6] I. Khalifa, A. Nawaz, R. Sobhy, S.A. Althawb, H. Barakat, Polyacylated anthocyanins constructively network with catalytic dyad residues of 3CLpro of 2019-nCoV than monomeric anthocyanins: a structural-relationship activity study with 10 anthocyanins using in-silico approaches, J. Mol. Graph. Model. 10 (2020) 76–90.
[7] S. Kim, D.M. Kim, B. Lee, Insufficient Sensitivity of RNA Dependent RNA Polymerase Gene of SARS-CoV-2 Viral Genome as Confirmatory Test Using Korean COVID-19 Cases, 2020.
[8] V. Moorthy, A.M.H. Restrepo, M.P. Preziosi, S. Swaminathan, Data sharing for novel coronavirus (COVID-19), Bull. World Health Organ. 98 (2020) 150.
[9] R. Singh, V.K. Bhardwaj, R. Purohit, Inhibition of nonstructural protein 15 of SARS-CoV-2 by golden spice: a computational insight, Cell Biochem. Funct. 40 (8) (2022 Dec) 926–934, https://doi.org/10.1002/cbf.3753. Epub 2022 Oct 6. PMID: 36203381; PMCID: PMC9874790.
[10] R. Singh, V.K. Bhardwaj, J. Sharma, R. Purohit, S. Kumar, In-silico evaluation of bioactive compounds from tea as potential SARS-CoV-2 nonstructural protein 16 inhibitors, J Tradit Complement Med 12 (1) (2022 Jan) 35–43, https://doi.org/10.1016/j.jtcme.2021.05.005. Epub 2021 Jun 3. PMID: 34099976; PMCID: PMC8172245.
[11] V.K. Bhardwaj, R. Singh, J. Sharma, V. Rajendran, R. Purohit, S. Kumar, Identification of bioactive molecules from tea plant as SARS-CoV-2 main protease inhibitors, J. Biomol. Struct. Dyn. 39 (10) (2021 Jul) 3449–3458, https://doi.org/10.1080/07391102.2020.1766572. Epub 2020 May 20. PMID: 32397940; PMCID: PMC7256349.
[12] R. Singh, V.K. Bhardwaj, J. Sharma, D. Kumar, R. Purohit, Identification of potential plant bioactive as SARS-CoV-2 Spike protein and human ACE2 fusion inhibitors, Comput. Biol. Med. 136 (2021 Sep), 104631, https://doi.org/10.1016/j.compbiomed.2021.104631. Epub 2021 Jul 8. PMID: 34273770; PMCID: PMC8264305.

[13] R. Singh, V.K. Bhardwaj, R. Purohit, Potential of turmeric-derived compounds against RNA-dependent RNA polymerase of SARS-CoV-2: an in-silico approach, Comput. Biol. Med. 139 (2021 Dec), 104965, https://doi.org/10.1016/j.compbiomed.2021.104965. Epub 2021 Oct 22. PMID: 34717229; PMCID: PMC8532373.

[14] Y. Aoyama, T. Katayama, M. Yamamoto, H. Tanaka, K. Kon, A new antitumor antibiotic product, demethylchartreusin. Isolation and biological activities, J. Antibiot. 45 (1992) 875–878.

[15] M. Iranshahi, A. Askari, A. Sahebkar, D. Hadjipavlou-Litina, Evaluation of antioxidant, anti-inflammatory and lipoxygenase inhibitory activities of the prenylated coumarin umbelliprenin, Daru 17 (2009) 99–103.

[16] N.B. Piller, A comparison of the effectiveness of some anti inflammatory drugs on thermal oedema, Br. J. Exp. Pathol. 56 (1975) 554–560.

[17] E.D. Kharasch, D.C. Hankins, J.K. Taraday, Single-dose methoxsalen effects on human cytochrome P-450 2A6 activity, Drug Metab. Dispos. 28 (2000) 28–33.

[18] T.C. McKee, R.W. Fuller, C.D. Covington, et al., New pyrano coumarins isolated from *Calophyllumlanigerum* and *Calophyllumteysmannii*, J. Nat. Prod. 59 (1996) 754–758.

[19] G. Steinkamp, H. Lindemann, Noscapine for the treatment of non-productive cough, Atemwegs Und Lungenkrankheiten 34 (5) (2008) 163.

[20] R.K. Meher, M.R. Naik, B. Bastia, P.K. Naik, Comparative evaluation of anti-angiogenic effects of noscapine derivatives, Bioinformation 14 (5) (2018) 236.

[21] L.D. Mendelsohn, ChemDraw 8 ultra, windows and macintosh versions, J. Chem. Inf. Comput. Sci. 44 (2004) 2225–2226.

[22] R.E. Ricketts, Practical optimization, philip E. Gill, walter murray and margret H. Wright, academic press inc.(london) limited, 1981. No. of pages: 401. ISBN: 0.12. 283950.1, Int. J. Numer. Methods Eng. 18 (1982), 954-954.

[23] T.A. Halgren, J. Comput. Chem. 20 (1999) 720–729.

[24] Z. Jin, X. Du, Y. Xu, et al., Structure of M^pro from SARS-CoV-2 and discovery of its inhibitors, Nature 582 (2020) 289–293. https://doi.org/10.1038/s41586-020 -2223-y.

[25] A. Onufriev, D. Bashford, D.A. Case, Modification of the generalized born model suitable for macromolecules, J. Phys. Chem. B 104 (2000) 3712–3720.

[26] P. Banerjee, A.O. Eckert, A.K. Schrey, R. Preissner, ProTox-II: a webserver for the prediction of toxicity of chemicals, Nucleic Acids Res. 46 (W1) (2018) W257–W263.

[27] U. Schmidt, S. Struck, B. Gruening, I.S. Jaeger, R. Parol, R. Preissner, SuperToxic: a comprehensive database of toxic compounds, Nucleic Acids Res. 37 (2009) 295–299.

[28] N.M. O'Boyle, M. Banck, C.A. James, C. Morley, T. Vandermeersch, G. R. Hutchison, Open Babel: an open chemical toolbox, J. Cheminf. 3 (2011) 33.

[29] L.L.C. Molsoft, 3366, North Torrey Pines Court, Suite 300, 2007. La Jolla, CA 92037, USA.

[30] S. Jo, T. Kim, V.G. Iyer, W. Im, CHARMM-GUI: a web-based graphical user interface for CHARMM, J. Comp.Chem. 29 (11) (2008) 1859–1865.

[31] G.R. Pereira, A.N. Da Silva, S.S. Do Nascimento, J.F. De Mesquita, In silico analysis and molecular dynamics simulation of human superoxide dismutase 3 (SOD3) genetic variants, J. Cell. Biochem. 120 (3) (2019) 3583–3598.

[32] J. Wang, et al., Automatic atom type and bond type perception in molecular mechanical calculations, J. Mol. Graph. Model. 25 (2006) 247–260, https://doi.org/10.1016/j.jmgm.2005.12.005.

[33] K. Lindorff-Larsen, et al., Improved side-chain torsion potentials for the Amber ff99SB protein force field, Proteins Struct. Funct. Genet. 78 (2010) 1950–1958, https://doi.org/10.1002/prot.22711.

[34] A.W. Sousa da Silva, W.F. Vranken, ACPYPE-Antechamber python parser interface, *BMC Res.* Notes 5 (2012) 1–8, https://doi.org/10.1186/1756-0500-5-367 Sousa.

[35] S. Kashefolgheta, A.V. Verde, Developing force fields when experimental data is sparse: AMBER/GAFF-compatible parameters for inorganic and alkyl oxoanions, Phys. Chem. Chem. Phys. 19 (2017) 20593–20607, https://doi.org/10.1039/C7CP02557B.

[36] P. Mark, L. Nilsson, Structure and dynamics of the TIP3P, SPC, and SPC/E water models at 298 K, J. Phys Chem A 105 (43) (2001) 9954–9960.

[37] T. Darden, D. York, L. Pedersen, Particle mesh Ewald: an N· log (N) method for Ewald sums in large systems, J. Chem. Phys. 98 (1993) 10089–10092, https://doi.org/10.1063/1.464397.

[38] H.J.C. Berendsen, J.P.M. Postma, W.F. van Gunsteren, A. DiNola, J.R. Haak, Molecular dynamics with coupling to an external bath, J. Chem. Phys. 81 (1984) 3684–3690.

[39] S. Borkotoky, A.A. Murali, Computational assessment of pH-dependent differential interaction of T7 lysozyme with T7 RNA polymerase, BMC Struct. Biol. 17 (1) (2018), 1-1.

[40] B. Hess, H. Bekker, H.J. Berendsen, J.G. Fraaije, LINCS: a linear constraint solver for molecular simulations, J. Comput. Chem. 18 (12) (1997) 1463–1472.

[41] B.R. Brooks, C.L. Brooks III, A.D. Mackerell Jr., L. Nilsson, R.J. Petrella, B. Roux, Y. Won, G. Archontis, C. Bartels, S. Boresch, A. Caflisch, CHARMM: the biomolecular simulation program, J. Comput. Chem. 30 (10) (2009) 1545–1614.

[42] A.T. Ayoub, M.A. Elrefaiy, K. Arakawa, Computational prediction of the mode of binding of antitumor lankacidin C to tubulin, ACS Omega 4 (2019) 4461–4471, https://doi.org/10.1021/acsomega.8b03470.

[43] Showkat Ahmad Mir, Auwal Muhammad, Archana Padhiary, Nirius Jenen Ekka, Iswar Baitharu, Pradeep Kumar Naik, Binata Nayak, Identification of potent EGFR-TKD inhibitors from NPACT database through combined computational approaches, J. Biomol. Struct. Dyn. (2023), https://doi.org/10.1080/07391102.2023.2171133.

[44] R. Kumari, Kumar, open source drug discovery consortium and lynn, g_mmpbsa A GROMACS tool for high-throughput MM-PBSA calculations, J. Chem. Inf. Model. 54 (2014) 1951–1962, https://doi.org/10.1021/ci500020m.

[45] K.A. Kumar, M. Sharma, V. Dalal, V. Singh, S. Tomar, P. Kumar, Multifunctional inhibitors of SARS-CoV-2 by MM/PBSA, essential dynamics, and molecular dynamic investigations, J. Mol. Graph. Model. 107 (2021 Sep 1), 107969.

[46] V.K. Bhardwaj, R. Singh, P. Das, R. Purohit, Evaluation of acridinedione analogs as potential SARS-CoV-2 main protease inhibitors and their comparison with repurposed anti-viral drugs, Comput. Biol. Med. 128 (2021 Jan), 104117, https://doi.org/10.1016/j.compbiomed.2020.104117. Epub 2020 Nov 12. PMID: 33217661; PMCID: PMC7659809.

[47] R. Spezia, et al., The effect of protein conformational flexibility on the electronic properties of a chromophore, Biophys. J. 84 (2003) 2805–2813, https://doi.org/10.1016/S0006-3495(03)70010-1.

[48] Showkat Ahmad Mir, Binata Nayak, Exploring binding stability of hydroxy-3-(4-hydroxyphenyl)-5-(4-nitrophenyl)-5, 5a, 7, 8, 9, 9a-hexahydrothiazolo [2, 3-b] quinazolin-6-one with T790M/L858R EGFR-TKD, J. Biomol. Struct. Dyn. (2022) 1–15.

[49] M.L. Holshue, C. DeBolt, S. Lindquist, K.H. Lofy, J. Wiesman, H. Bruce, G. Diaz, First case of 2019 novel coronavirus in the United States, N Engl J Med. 382 (2020) 929–936, https://doi.org/10.1056/NEJMoa2001191.

[50] J. Cohen, Can an anti-HIV combination or other existing drugs outwit the new coronavirus, Science 10 (2020).

[51] Xueting Yao, Fei Ye, Miao Zhang, Cheng Cui, Baoying Huang, Peihua Niu, Xu Liu, et al., In vitro antiviral activity and projection of optimized dosing design of hydroxychloroquine for the treatment of severe acute respiratory syndrome coronavirus 2 (SARS-CoV-2), Clin. Infect. Dis. 71 (15) (2020) 732–739.

[52] Pranab Kishor Mohapatra, Sambhav Chopdar Kumar, Ganesh Chandra Dash, Abhay Kumar Mohanty, and Mukesh Kumar Raval. "In silico screening and covalent binding of phytochemicals of Ocimum sanctum against SARS-CoV-2 (COVID 19) main protease, J. Biomol. Struct. Dyn. (2021) 1–10.

[53] P. Kumar, T. Bhardwaj, A. Kumar, N. Garg, R. Giri, One microsecond MD simulations of the SARS-CoV-2 main protease and hydroxychloroquine complex reveal the intricate nature of binding, J. Biomol. Struct. Dyn. 40 (21) (2022) 10763–10770, https://doi.org/10.1080/07391102.2021.1948447. Epub 2021 Jul 29. PMID: 34320905.

[54] K.T. Choy, A.Y. Wong, P. Kaewpreedee, S.F. Sia, D. Chen, K.P.Y. Hui, D.K.W. Chu, M.C.W. Chan, P.P. Cheung, X. Huang, M. Peiris, H.L. Yen, Remdesivir, lopinavir, emetine, and homoharringtonine inhibit SARS-CoV-2 replication in vitro, Antivir. Res. 178 (2020 Jun), 104786, https://doi.org/10.1016/j.antiviral.2020.104786. Epub 2020 Apr 3. PMID: 32251767; PMCID: PMC7127386.

[55] D. Paul, D. Basu, S. Ghosh Dastidar, Multi-conformation representation of Mpro identifies promising candidates for drug repurposing against COVID-19, J. Mol. Model. 27 (5) (2021 Apr 17) 128, https://doi.org/10.1007/s00894-021-04732-1. PMID: 33864532; PMCID: PMC8052536.

[56] M.N. Drwal, P. Banerjee, M. Dunkel, M.R. Wettig, R. Preissner, ProTox: a web server for the in silico prediction of rodent oral toxicity, Nucleic Acids Res. 42 (2014) 53–58.

[57] H.L. Nguyen, N.Q. Thai, D.T. Truong, M.S. Li, Remdesivir strongly binds to both RNA-dependent RNA polymerase and main protease of SARS-CoV-2: evidence from molecular simulations, J. Phys. Chem. B 124 (50) (2020) 11337–11348.

[58] Lobanov Miu, N.S. Bogatyreva, O.V. Galzitskaia, [Radius of gyration is indicator of compactness of protein structure], Mol Biol (Mosk) 42 (4) (2008 Jul-Aug) 701–706. Russian. PMID: 18856071.

[59] J. Roshni, R. Vaishali, K.S. Ganesh, N. Dharani, K.J. Alzahrani, H.J. Banjer, S. Patil, Multi-target potential of Indian phytochemicals against SARS-CoV-2: A docking, molecular dynamics and MM-GBSA approach extended to Omicron B.1.1. 529, Journal of infection and public health 15 (6) (2022) 662–669.

[60] P.K. Parida, D. Paul, D. Chakravorty, The natural way forward: molecular dynamics simulation analysis of phytochemicals from Indian medicinal plants as potential inhibitors of SARS-CoV-2 targets, Phytother Res. 34 (12) (2020) 3420–3433.

[61] M. Gogoi, M. Borkotoky, S. Borchetia, P. Chowdhury, S. Mahanta, A.K. Barooah, Black tea bioactives as inhibitors of multiple targets of SARS-CoV-2 (3CLpro, PLpro and RdRp): a virtual screening and molecular dynamic simulation study, J. Biomol. Struct. Dyn. 40 (15) (2022) 7143–7166.